An Illumination Model for a Skin Layer Bounded by Rough Surfaces

Jos Stam
Alias | wavefront
1218 Third Ave, 8th Floor,
Seattle, WA 98101

Abstract

In this paper we present a novel illumination model that takes into account multiple anisotropic scattering in a layer bounded by two rough surfaces. We compute the model by a discrete-ordinate solution of the equation of radiative transfer. This approach is orders of magnitude faster than a Monte Carlo simulation and does not suffer from any noisy artifacts. By fitting low order splines to our results we are able to build analytical shaders. This is highly desirable since animators typically want to texture map the parameters of such a shader for higher realism. We apply our model to the important problem of rendering human skin. Our model does not seem to have appeared before in the optics literature. Most previous models did not handle rough surfaces at the skin's boundary. Also we introduce a novel analytical bidirectional transmittance distribution function (BTDF) for an isotropic rough surface by generalizing the Cook-Torrance model. We believe our work to be both of practical and theoretical importance.

Keywords:
Illumination. Illumination Effects. Reflectance & Shading Models.

1 Introduction

The work described in this paper was motivated by the desire to model the appearance of human skin under various lighting conditions. A good model for the reflection of light from skin has many obvious applications in the entertainment industry, where there is a keen interest in making virtual actors appear more life-like. However, despite the importance of this problem there are very few analytical models that convincingly model the appearance of skin. This is probably because the interaction of light with human skin is a very complicated physical phenomenon. Skin appearance depends not only on the skin's surface but also on the layer directly below it: incoming light is not only reflected specularly (as in oily shiny skin) but is also scattered diffusely within the flesh. This explains why traditional Phong-like surface-based reflection models fail to capture the subtle appearance of skin. Most traditional models approximate the contributions due to the subsurface layer inadequately using a Lambertian cosine term. A good model for subsurface scattering is also important to model substances other than human skin such as paints and tissues. An effective skin reflection model should ideally depend analytically on a set of meaningful parameters, such as the

skin's surface roughness and amount of melanin. Animators typically want to texture map these parameters to add visual detail, such as freckles, pores or a shiny forehead.

In this paper we propose a new model for subsurface reflections based on linear transport theory. This theory has matured well and has been applied to a wide range of disciplines, including nuclear physics, the atmospheric sciences, astrophysics and computer graphics. It seems that the only transport theoretical model for subsurface scattering in computer graphics is the one proposed by Hanrahan and Krueger [5]. They introduce an analytical model for layers that only scatter weakly using the single-scattering approximation. In addition, they assume a perfectly smooth reflecting and refracting surface at the top of the layers. These approximations are, however, ill suited for skin, since the skin's surface is rarely perfectly smooth and multiple scattering is very important. To address the latter problem, Hanrahan and Krueger ran a Monte Carlo simulation to precompute reflection maps for different configurations of sub-layers. Unfortunately, the Monte Carlo method converges very slowly, so handling a wide range of interesting skin parameters requires huge amounts of data to be computed. Because the model of Hanrahan and Krueger did not satisfy our needs, we decided to derive our own model in a more general setting.

We first turned to the abundant literature on the subject from other fields. Most relevant to our problem is the literature in the medical sciences studying the optics of skin for such applications as non-invasive surgery. We first consulted the review articles [23] and [24]. The latter article discusses an approximation which is too coarse for our purposes. The first reference from a Russian journal only mentions Monte Carlo methods and the so-called adding-doubling method. We have already drawn attention to the drawbacks of the Monte Carlo approach. The adding-doubling technique was used by Prahl and co-workers to extract parameters from skin measurement [18] and is based on earlier work in astronomy [6]. This technique, however, is iterative in nature and does not handle rough surface boundaries. At this point we turned to the atmospheric sciences. The problem addressed there is how to compute the global interchange of radiation between the atmosphere and the ocean. The ocean is very much like skin since it has a rough boundary and light is scattered below it. We found a very attractive model based on the discrete-ordinate approximation of radiative transfer [3]. In particular, Stamnes and co-workers developed a general solution framework for the atmosphere-ocean radiative problem [8, 21]. Unfortunately their model does not handle rough surfaces. It seems that the "state of the art" model in this area resorts to a Monte Carlo simulation to determine the effect of a rough surface [14].

After this review, we decided to extend the discrete-ordinate approach of Jin and Stamnes [8] to include rough surfaces. We first required a good analytical model for the Bidirectional Transmittance Distribution Function (BTDF). We are aware of only one such model in computer graphics based on the wave theory of light [7]. Unfortunately this model is fairly complex, so we derive a simpler one in this paper for the first time. Our model is an extension of the BRDFs of Cook-Torrance [4] and of van Ginneken et al. [25]. Extending a reflectance model to include transmittance may seem straightforward at first, but we encountered some subtle issues. The first contribution of this paper is to resolve these issues. The second contribution is a general discrete-ordinate solution for a scattering layer bounded by rough surfaces. Our model is, therefore, of interest to computer graphics and potentially to other fields. We show how to efficiently solve the problem by a suitable "diagonalization" of the "transfer matrix." We use the machinery of Fourier transforms and eigenanalysis to perform this task. To build practical reflection models for computer graphics, we fit low-order splines to our discretized functions. Our approach is orders of magnitude faster than Monte Carlo methods, requires less memory, and does not suffer from any noisy artifacts. The parameters of our model can also be texture mapped without the need for

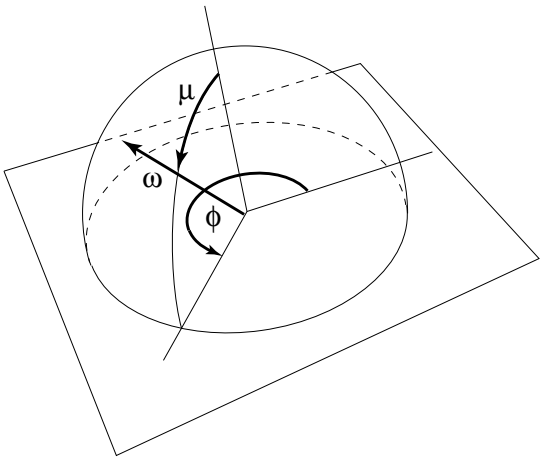

Figure 1: Definition of a direction $\omega = (\mu, \phi)$.

any recomputations. It is therefore ideally suited for an implementation as a shader in a standard rendering package.

We briefly mention here that the discrete-ordinate method has been used before in a different context in computer graphics. Both Max and Languenou et al. used this technique to compute the scattering in non-constant densities such as clouds [11, 13]. Their methods, however, do not lead to analytical reflection models since they consider arbitrary densities. They also do not address the problem of rough surfaces refracting and reflecting light at the boundaries. The same comments apply to the method of Kajiya and Von Herzen [9] and the radiosity-based approach of Rushmeier et al. [20].

The rest of the paper is organized as follows. The next section details the physics involved and introduces the equivalent discrete problem. In Section 3 we show how to solve the discrete problem efficiently. Section 4 presents a derivation of our new BTDF. Section 5 clarifies many implementation issues and discusses the corresponding "skin shader". In Section 6 we present some results and compare them to experimental data, while in Section 7 we conclude and discuss future research. Material of a rather technical nature is addressed in the appendices.

1.1 Notational Preliminaries

Much of the material in this paper can be presented more elegantly using a "matrix operator approach" [17]. Many relations are expressed more compactly without indices in vector and matrix form. In this paper all vectors are denoted by bold lowercase characters: $\mathbf{v}$. The elements of $\mathbf{v}$ are denoted by the corresponding italicized letter: v_i is the i-th component of $\mathbf{v}$. An element of a vector should not be confused with an indexed vector such as $\mathbf{v}_k$. A matrix is denoted by a bold upper case character such as $\mathbf{M}$ and its elements are denoted by $M_{i,j}$. The transpose of $\mathbf{M}$ is written $\mathbf{M}^T$.

2 Discretizing the Physics

2.1 Physical parameters

The physical quantity corresponding to a visual stimulus is the radiance u. This quantity has units of power per unit area per unit solid angle and gives the amount of radiant power flowing from a particular position in a particular direction. Following Hanrahan and Krueger [5] we assume that the skin depth is along the z-direction and that the skin's properties are uniform in each xy-plane. In this setting it is more convenient to use the dimensionless optical depth τ rather than the depth z, where

$$\tau = z/L$$

and L is the mean free path of a photon in the medium. Consequently, the radiance is a function of optical depth and direction. We represent a direction by an ordered pair $\pm\omega = (\pm\mu, \phi)$ where $\mu = \cos\theta$ is the cosine of the elevation angle θ and ϕ is the azimuthal angle (see Figure 1). In the following we always assume that the cosine $\mu \geq 0$. We therefore denote a downward direction by $-\omega = (-\mu, \phi)$. The use of the minus sign is purely notational in this context.

The optical properties of the skin are modeled by two parameters that describe how light scatters at each point. They are the albedo Ω and the anisotropy factor g. The albedo gives the fraction of light that is scattered versus absorbed and is typically close to one for skin. The distribution of scattered light is defined by a phase function p. This function gives the probability that a photon travelling in a direction ω' is scattered in another direction ω. We rely on the *Henyey-Greenstein phase function*, a useful model frequently seen in the optics literature:

$$p(\omega', \omega) = \frac{1 - g^2}{(1 + g^2 - 2g\cos\gamma)^{3/2}}.$$

Here γ is the angle between the directions ω' and ω. The anisotropy factor $g \in [0, 1]$ models how much light is scattered forward. For $g = 0$ the medium scatters isotropically, while for $g = 1$ the scattering is in the forward direction only. Scattering in skin is typically highly anisotropic with values of g in the range $[0.7, 0.95]$. Both the albedo and the anisotropy factor of skin depend on depth and wavelength. It is interesting that the popularity of the Henyey-Greenstein phase function stems from the fact that it has a very simple expansion in terms of the associated Legendre functions (see Appendix C). This is rarely mentioned in the computer graphics literature. The expansion coefficients are the powers of g. The higher the anisotropy, the more terms are required in the expansion. We associate with the phase function a linear scattering functional:

$$\mathcal{S}\{u\}(\tau, \omega) = \frac{\Omega}{4\pi} \int_{4\pi} p(\omega', \omega) u(\tau, \omega')\, d\omega', \tag{1}$$

where the integration is over all possible directions.

The reflection and refraction at the skin's boundaries are modeled as isotropic rough surfaces. In our model we assume that the skin has a uniform index of refraction n_2 and is bounded above and below by media having indices equal to n_1 and n_3, respectively. To model the reflection, we use a variant of the Cook-Torrance model [4] proposed by van Ginneken et al. [25]. For the transmission we derive a new model in Section 4 since we could not find a satisfactory one in the optics literature. Both the transmission and reflection models depend on a roughness parameter σ. The BRDF and BTDF are denoted by $r_{ij}(\omega, \omega')$ and $t_{ij}(\omega, \omega')$, respectively, for light coming from

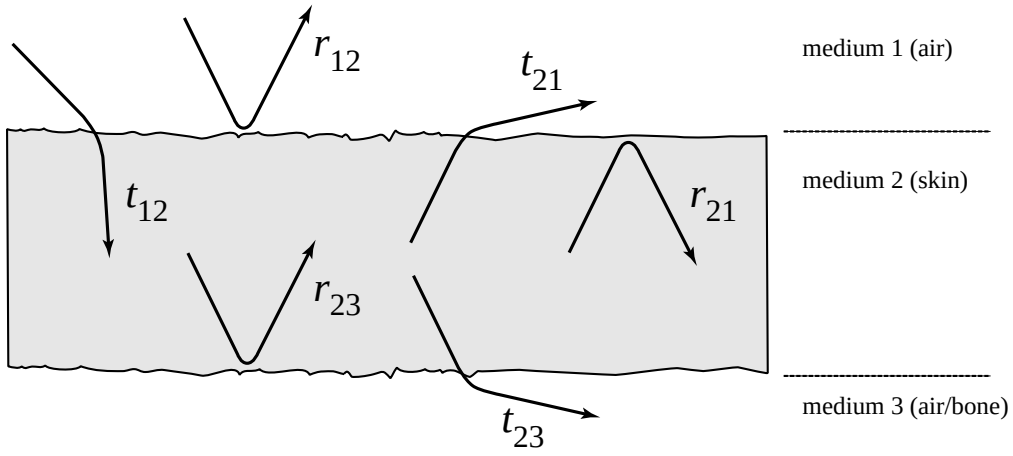

Figure 2: Nomenclature for the BRDFs and BTDFs.

material $i \in 1, 2, 3$ arriving at material $j \in 1, 2, 3$, where, for example, r_{12} models the reflection off of the top surface. This nomenclature is clarified in Figure 2. We associate with these distributions linear reflection and transmission operators:

$$\mathcal{R}_{ij}\{u\}(\tau, \pm\omega) = \int_{2\pi} r_{ij}(\mp\omega', \pm\omega) u(\tau, \mp\omega') \mu' \, d\omega', \tag{2}$$

$$\mathcal{T}_{ij}\{u\}(\tau, \pm\omega) = \int_{2\pi} t_{ij}(\pm\omega', \pm\omega) u(\tau, \pm\omega') \mu' \, d\omega', \tag{3}$$

where the integration is over the positive hemisphere and the signs depend on the BRDF or BTDF considered, e.g., r_{12} has opposite signs from r_{21} as is evident from Figure 2.

2.2 Equation of Transfer

An equation for the radiance within the skin is obtained by considering its variation in an infinitesimal cylinder aligned with the direction ω. The change is equal to the amount of light scattered into this direction minus the light absorbed and scattered out of this direction:

$$-\mu \frac{du}{d\tau} = -u + \mathcal{S}\{u\}, \tag{4}$$

where $\mathcal{S}$ is the scattering operator defined in Equation 1. To completely specify the problem, this equation requires boundary conditions at the top and the bottom of the skin layer. At the skin's surface ($\tau = 0$) the downwelling radiance is equal to the transmitted radiance plus the internal reflections of the radiance coming from the internal layer:

$$u(0, -\omega) = t_{12}(-\omega_0, -\omega) + \mathcal{R}_{21}\{u\}(0, -\omega). \tag{5}$$

Similarly, if we assume there are no sources below the skin, the upwelling radiance at the bottom of the layer ($\tau = \tau_b$) is given by

$$u(\tau_b, \omega) = \mathcal{R}_{23}\{u\}(\tau_b, \omega). \tag{6}$$

Once Equation 4 is solved using these boundary conditions, the BRDF and the BTDF due to scattering in the skin's layer are equal to

$$r_s(-\omega_0, \omega) = \mathcal{T}_{21}\{u\}(0, \omega)/\mu_0 \quad \text{and} \quad t_s(-\omega_0, -\omega) = \mathcal{T}_{23}\{u\}(\tau_b, -\omega)/\mu_0,$$

respectively. In addition, the reflection due to an ambient light source of radiance is modeled by integrating the skin's BRDF over all incident directions $-\omega_0$:

$$r_a(\omega) = \int_{2\pi} r_s(-\omega_0, \omega)\ \mu_0\ d\mu_0.$$

The total amount of light reflected off the skin is the sum of the part directly reflected by the surface, the ambient term and the radiance leaving the subsurface layer:

$$r_{tot}(\omega) = r_{12}(-\omega_0, \omega) + r_a(\omega) + r_s(-\omega_0, \omega).$$

In Section 4 we provide a model for r_{12} (and the other r_{ij} and t_{ij}) while the next section describes a method of solution for r_s and t_s.

2.3 Angular Discretization

We discretize the angular part of Equation 4 in two steps. Because we assume that the surface roughness is isotropic and that the skin is horizontally uniform, we can decompose the azimuthal dependence of the radiance into a cosine series:

$$u(\tau, \omega) = \sum_{k=0}^{N} u_k(\tau, \mu) \cos k(\phi - \phi_0). \tag{7}$$

Next we discretize the cosines μ into $2M$ discrete samples (see Appendix A for how they are chosen):

$$\mu_1, \mu_2, \cdots, \mu_M, -\mu_1, -\mu_2, \cdots, -\mu_M. \tag{8}$$

These values are also known as "ordinates," hence the name "discrete-ordinates" to refer to this type of discretization. The corresponding values of the discretized radiances are stored in a $2M$ vector

$$\mathbf{u}_k(\tau) = (u_k(\tau, \mu_1), \cdots, u_k(\tau, -\mu_M))^T \qquad k = 0, \cdots, N.$$

As shown in Appendix A, the scattering operator in Equation 4 is discretized into a collection of $N + 1$ matrices $\mathbf{S}_k$ ($k = 0, \cdots, N$), each of size $2M \times 2M$. These discretizations convert the transfer equation into $N + 1$ decoupled linear ordinary differential vector equations:

$$-\mathbf{W}\frac{d\mathbf{u}_k(\tau)}{d\tau} = -\mathbf{u}_k(\tau) + \mathbf{S}_k\mathbf{u}_k(\tau),$$

where $\mathbf{W}$ is a diagonal matrix containing the samples of Equation 8. The last equation can be written more compactly as

$$\frac{d\mathbf{u}_k(\tau)}{d\tau} = \mathbf{M}_k\mathbf{u}_k(\tau), \tag{9}$$

where $\mathbf{M}_k = \mathbf{W}^{-1}(\mathbf{I} - \mathbf{S}_k)$ and $\mathbf{I}$ is the identity matrix. Equation 9 is the main equation of this paper. In the next section we show how to solve it efficiently.

3 Direct Solution of the Discrete Problem

This section is inspired by the work of Jin and Stamnes [8]. However, our compact vector/matrix notation greatly simplifies the presentation. Our approach is also more general, since we consider surfaces of arbitrary roughness at the boundaries.

3.1 Diagonalization

We assume that the skin is composed of a layer with constant optical properties sandwiched between two isotropic rough surfaces. In order to simplify the notation in this section, we will drop the dependence of all quantities on the index "k". This is justified because the equations for different terms in the cosine expansion are entirely decoupled. In the skin the radiance satisfies the following equation:

$$\frac{d\mathbf{u}(\tau)}{d\tau} = \mathbf{M}\mathbf{u}(\tau).$$

Ignoring the boundary conditions for the moment, we see that this is a homogeneous vector ordinary differential equation. Such an equation is solved efficiently by putting the matrix $\mathbf{M}$ into diagonal form. Indeed, in diagonal form the equations are decoupled and can be solved analytically. Diagonalizing $\mathbf{M}$ is equivalent to computing its eigenvalues and eigenvectors:

$$\mathbf{M} = \mathbf{V}\mathbf{\Lambda}\mathbf{V}^{-1}.$$

Here $\mathbf{\Lambda}$ is a diagonal matrix containing the eigenvalues of $\mathbf{M}$:

$$\mathbf{\Lambda} = \mathrm{diag}\,(\lambda_1, \cdots, \lambda_M, -\lambda_1, \cdots, -\lambda_M)$$

where $\lambda_i > 0$ for $i = 1, \cdots, M$ (see Appendix E) and $\mathbf{V}$ contains the eigenvectors stored columnwise. If we let $\mathbf{w}(\tau)$ be the transformed radiance $\mathbf{w} = \mathbf{V}^{-1}\mathbf{u}$, then

$$\frac{d\mathbf{w}(\tau)}{d\tau} = \mathbf{\Lambda}\mathbf{w}(\tau).$$

The exact solution to this differential equation is given by:

$$\mathbf{w}(\tau) = e^{\mathbf{\Lambda}\tau}\mathbf{u}_0, \tag{10}$$

where the exponential is simply the diagonal matrix whose elements are the exponential of the elements of $\mathbf{\Lambda}\tau$. The vector $\mathbf{u}_0$ in Equation 10 is to be determined from the boundary conditions. The radiance in the layer is then obtained by inverting our earlier transformation:

$$\mathbf{u}(\tau) = \mathbf{V}\mathbf{w}(\tau) = \mathbf{V}e^{\mathbf{\Lambda}\tau}\mathbf{u}_0. \tag{11}$$

Our next step is to find a vector $\mathbf{u}_0$ satisfying the boundary conditions.

3.2 Solving the Discrete Problem: Boundary conditions

We have just shown that the radiance in each layer can be solved for directly in terms of the eigenvectors and eigenvalues of the transfer matrix. We can rewrite Equation 11 separating the parts corresponding to upward and downward directions:

$$\begin{pmatrix} \mathbf{u}^+(\tau) \\ \mathbf{u}^-(\tau) \end{pmatrix} = \begin{pmatrix} \mathbf{V}^+ & \mathbf{V}^- \\ \mathbf{V}^- & \mathbf{V}^+ \end{pmatrix} \begin{pmatrix} \mathbf{E}(\tau)\mathbf{u}_0^+ \\ \mathbf{E}(-\tau)\mathbf{u}_0^- \end{pmatrix}, \tag{12}$$

where each of the $\mathbf{E}$ matrices contains half of the exponentials:

$$\mathbf{E}(t) = e^{\mathbf{\Lambda}^+ t}.$$

The goal in this section is to compute the unknown vectors $\mathbf{u}_0^+$ and $\mathbf{u}_0^-$ given by Equations 5 and 6. First, let $\mathbf{R}_{ij}$ and $\mathbf{T}_{ij}$ denote the discrete versions of $\mathcal{R}_{ij}$ and $\mathcal{T}_{ij}$ respectively. Since they are defined only over the positive hemisphere they are of size $M \times M$. The top and bottom boundary conditions in terms of these matrices are

$$\begin{aligned} \mathbf{u}^-(0) &= \mathbf{T}_{12}\mathbf{d}_0 + \mathbf{R}_{21}\mathbf{u}^+(0) \quad \text{and} \qquad (13) \\ \mathbf{u}^+(\tau_b) &= \mathbf{R}_{23}\mathbf{u}^-(\tau_b). \qquad (14) \end{aligned}$$

The vector $\mathbf{d}_0$ represents the incident radiances, and for a directional light source is zero for each entry except for the entry corresponding to $-\mu_0$ where it is equal to one. By substituting Equations 13 and 14 into Equation 12 and rearranging,

$$\begin{pmatrix} \mathbf{V}^- - \mathbf{R}_{21}\mathbf{V}^+ & \mathbf{V}^+ - \mathbf{R}_{21}\mathbf{V}^- \\ (\mathbf{V}^+ - \mathbf{R}_{23}\mathbf{V}^-)\,\mathbf{E}(\tau_b) & (\mathbf{V}^- - \mathbf{R}_{23}\mathbf{V}^+)\,\mathbf{E}(-\tau_b) \end{pmatrix} \begin{pmatrix} \mathbf{u}_0^+ \\ \mathbf{u}_0^- \end{pmatrix} = \begin{pmatrix} \mathbf{T}_{12}\mathbf{d}_0 \\ \mathbf{0} \end{pmatrix}.$$

This system, however, is ill-conditioned because the matrix $\mathbf{E}(\tau_b)$ has entries that grow exponentially with τ_b. Fortunately, we can easily fix this problem by setting $\mathbf{u}_0^+ = \mathbf{E}(-\tau_b)\tilde{\mathbf{u}}_0^+$ and solving for $(\tilde{\mathbf{u}}_0^+, \mathbf{u}_0^-)$ instead [21]. The new system becomes:

$$\begin{pmatrix} (\mathbf{V}^- - \mathbf{R}_{21}\mathbf{V}^+)\,\mathbf{E}(-\tau_b) & \mathbf{V}^+ - \mathbf{R}_{21}\mathbf{V}^- \\ \mathbf{V}^+ - \mathbf{R}_{23}\mathbf{V}^- & (\mathbf{V}^- - \mathbf{R}_{23}\mathbf{V}^+)\,\mathbf{E}(-\tau_b) \end{pmatrix} \begin{pmatrix} \tilde{\mathbf{u}}_0^+ \\ \mathbf{u}_0^- \end{pmatrix} = \begin{pmatrix} \mathbf{T}_{12}\mathbf{d}_0 \\ \mathbf{0} \end{pmatrix}. \qquad (15)$$

This linear system is well behaved and can be solved using any standard linear solver. Once the solution is obtained, the upward radiance at the top and the downward radiance at the bottom of the layer are given by:

$$\begin{aligned} \mathbf{u}^+(0) &= \mathbf{V}^+\mathbf{E}(-\tau_b)\tilde{\mathbf{u}}_0^+ + \mathbf{V}^-\mathbf{u}_0^- \qquad \text{and} \\ \mathbf{u}^-(\tau_b) &= \mathbf{V}^-\tilde{\mathbf{u}}_0^+ + \mathbf{V}^+\mathbf{E}(-\tau_b)\mathbf{u}_0^-, \end{aligned}$$

respectively. These are the radiances just inside the rough surfaces of the skin layer. To compute the radiances exiting the surface, we have to multiply these radiances by the transmission matrices $\mathbf{T}_{21}$ and $\mathbf{T}_{23}$, respectively:

$$\mathbf{u}_r = \mathbf{T}_{21}\mathbf{u}^+(0) \quad \text{and} \quad \mathbf{u}_t = \mathbf{T}_{23}\mathbf{u}^-(\tau_b). \qquad (16)$$

3.3 Summary

First we restore the subscript "k" to indicate that the radiances of Equation 16 correspond to a single term in the cosine series. Consequently, the complete description of the radiances is given by the following vectors

$$\mathbf{u}_{r,0}, \cdots, \mathbf{u}_{r,N} \quad \text{and} \quad \mathbf{u}_{t,0}, \cdots, \mathbf{u}_{t,N}.$$

These radiances are for a particular incoming direction $-\omega_0 = (-\mu_0, 0)$. To get a discrete description of the BRDF r_s of the skin layer we sample the incoming directions at the ordinates $\mu_1, \cdots, \mu_M$. The discrete representation of the BRDF is, therefore, a collection of $N+1$ matrices $\mathbf{R}_k$ of size $M \times M$ ($k = 0, \cdots, N$). The i-th column of this matrix consists of the vector $\mathbf{u}_{r,k}$ computed for the incident direction $(-\mu_i, 0)$, $i = 1, \cdots, M$. In a similar fashion we build a set of matrices $\mathbf{T}_k$ for the BTDF t_s of the skin layer ($k = 0, \cdots, N$). A high level description of the algorithm that computes these matrices is given in Figure 3.

ComputeRT:
    For $k = 0, \cdots, N$ do
        Compute the scattering matrix $\mathbf{M}_k$ (Appendix A)
        Compute the reflection and transmission matrices $\mathbf{R}_{ij}$ and $\mathbf{T}_{ij}$ (Appendix D)
        Compute eigenstructure of $\mathbf{M}_k$ (see Appendix E)
        For $i = 1, \cdots, M$
            Solve linear system for incoming direction μ_i (Equation 15)
            Transmit radiances out of the layer (Equation 16)
            Set the i-th columns of $\mathbf{R}_k$ and $\mathbf{T}_k$
        next
    next

Figure 3: Summary of our algorithm.

parameter	num. of samples	samples									
T	10	0.0	0.1	0.2	0.3	0.4	0.5	0.6	0.7	0.8	0.9
σ	9	0.1	0.2	0.3	0.4	0.5	0.6	0.7	0.8	0.9	
Ω	7	0.1	0.5	0.75	0.8	0.9	0.999	1.0			
g	10	0.0	0.1	0.2	0.3	0.4	0.5	0.6	0.7	0.8	0.9

Table 1: Samples used for each of our parameters.

We have precomputed these matrices for different values of the parameters that model the skin layer. These parameters are the transparency $T = e^{-\tau_b}$, the albedo Ω, the anisotropy factor g of the phase function, and the roughness σ of the surfaces bounding the skin layer. Each parameter is dimensionless and takes on values between zero and one. The precomputations were done for all possible combinations of the parameter values listed in Table 1. The ratio of the indices of refraction is kept constant throughout: it is set to 1.4, roughly that of human skin. The number of ordinates M was determined from the discretizations of the BRDF and the BTDF of the skin's surface (derived in the next section). For a roughness $\sigma = 0.1$ we neededed $M = 30$ ordinates while for other values $M = 24$ was sufficient. The number of cosine series is always set to twice the number of ordinates: $N = 2M$ [8].

Because the scattering matrix depends only on Ω and g, we first computed the eigenstructures for all $7 \times 10 = 70$ possible values of the parameters. We used the `RG` routine from EISPACK [16] to compute the eigenvectors and eigenvalues. We encountered no numerical problems except when the albedo was exactly one. An easy fix is simply to set the albedo to a value almost equal to one, i.e., $\Omega = 0.999999$. Once the eigenstructures were available we used them to precompute the reflection r_s and transmission t_s of the skin layer for all possible combinations of the samples listed in Table 1. We used the routine `DGESL` from LINPACK to solve the linear system of Equation 15.

The precomputation generates a huge data set. Our next task was to compress the data using well chosen approximations. We first experimented with the elegant non-linear representation of Lafortune et al. [10]. We did get some good matches using three cosine lobes. However, in many cases the non-linear least square solver got stuck in local minima. For these reasons we adopted a less efficient but more straightforward compression scheme. First, not all cosine terms need to be included. For the reflection at the top of the layer we found that in general, 5

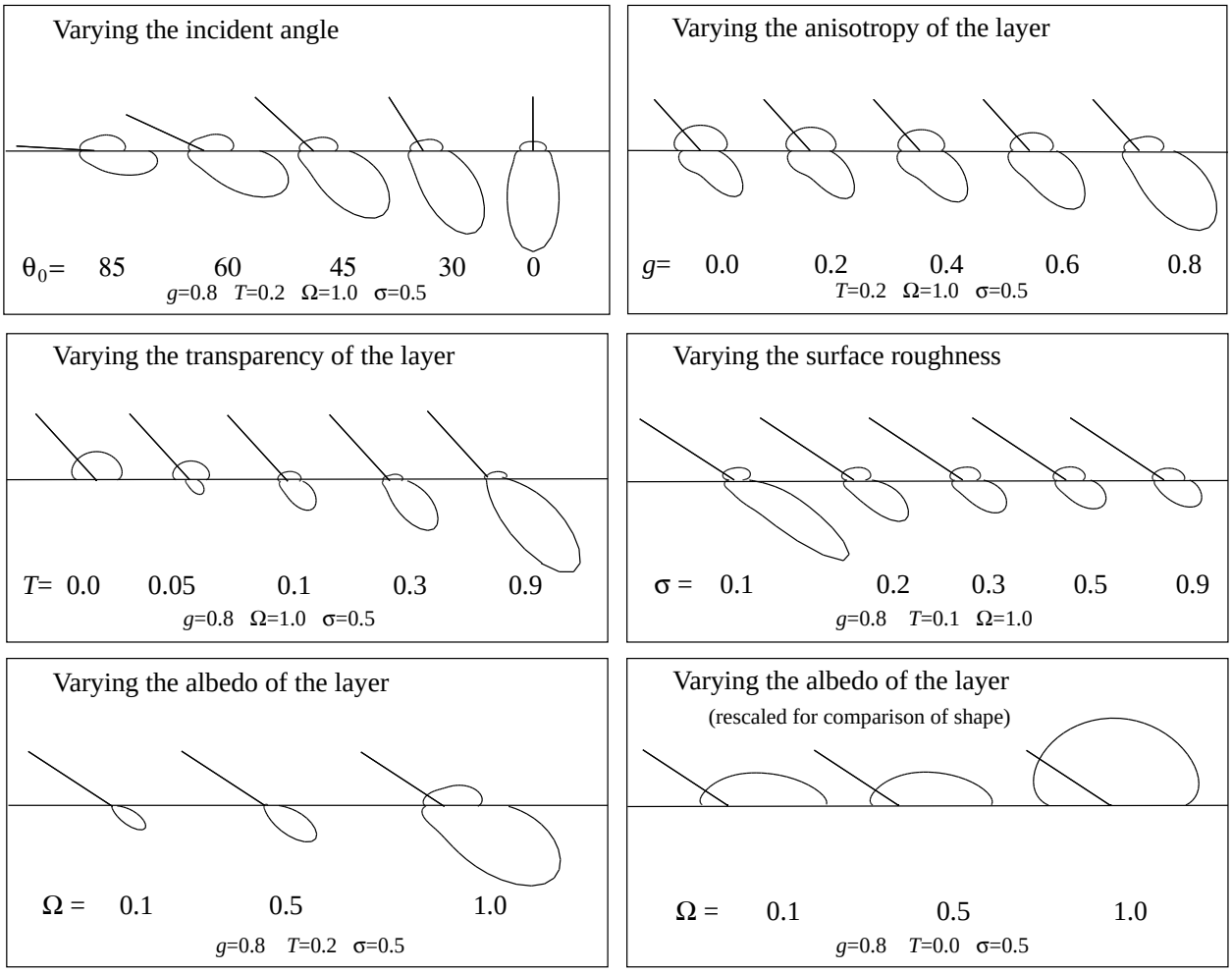

Figure 4: Cross-sections of the reflection and transmission functions of the skin layer for different values of the parameters.

terms ($N = 4$) were sufficient, while for the transmission at the bottom 15 ($N = 14$) terms were required. These numbers were obtained by visually comparing the data to the approximation. We further compressed the data by fitting a cubic Bezier surface to the data stored in the reflection (resp. transmission) matrix $\mathbf{R}_k$ (resp. $\mathbf{T}_k$). We constrained the control vertices to respect the symmetry of these matrices (Helmholtz reciprocity).

In Figure 4 we demonstrate the effect of our parameters on the reflection and transmission functions. The simple shapes of the lobes first led us to believe that they might be modeled by simple analytical expressions. The variation with each parameter is, however, quite subtle and none of our analytical estimations could handle all variations at the same time. Analytical solutions are rare when multiple scattering is included. Even the simplest case of a semi-infinite constant medium with isotropic scattering does not admit an analytical solution [3]. The distributions are clearly different from a simple constant Lambert term. The main difference is that the reflected lobe is flatter and has a bias towards the forward direction. This is consistent with some of the experimental data in [12]. Our distributions also vary from those of Hanrahan and Krueger [5]. Because they assumed a smooth surface, their distributions tend to zero for glancing angles. We get the same behavior asymptotically when the surface roughness tends to zero (see Figure 4). The

shape of their distributions corresponds to the plots with a low albedo in Figure 4.

To further validate our model we wrote a simple Monte Carlo simulator, compared the results for a set of different parameters and found good agreement. Of course we could not verify this for all possible values listed in Table 1 because of the inefficiency of the Monte Carlo technique.

4 Reflection and Refraction from Rough Surfaces

In this section we derive BRDF and BTDF models for an isotropic random rough surface. As in van Ginneken et al. [25] we derive these models directly from a statistical model of the height field. Indeed, our BRDF is essentially the same as theirs. Our main contribution is of course the new BTDF model. To the best of our knowledge, a similar model has not appeared before in the optics literature. We have chosen to derive the BRDF here as well for two reasons. First, it makes the derivation easier to follow. Second, since we need an explicit expression for the BRDF, it makes the paper self-contained.

We assume that our surface is an isotropic gaussian random height field [1]. The probability that a normal ω_a lies within an infinitesimal solid angle $d\omega_a = (d(\cos\theta_a), d\phi_a)$ is given by the Beckmann function [1]:

$$P(\omega_a)\ d\omega_a = \frac{1}{2\pi\sigma^2\cos^3\theta_a}\exp\left(-\frac{\tan^2\theta_a}{2\sigma^2}\right)\ d\omega_a, \tag{17}$$

where σ is the RMS slope of the surface. Let the surface be illuminated by a directional source of irradiance E_0 of direction $\omega_0 = (\cos\theta_0, \phi_0)$. For each direction ω_r, resp. ω_t, there is a unique normal ω_a that will reflect (resp. refract) the incoming light in the direction ω_r (resp. ω_t). In the case of reflection, this vector is simply the vector halfway between ω_0 and ω_r. For refraction it is the (normalized) vector equal to the sum of ω_0 and $\eta\omega_t$, where η is the ratio of the indices of refraction above and below the surface. Notice that η can be smaller than 1 when computing t_{21}, for example. In cases where $\eta > 1$ it's possible that no normal exists that refracts the incoming light in the direction ω_t. This happens whenever ω_t lies outside of the cone of refraction. In this case the BTDF is simply zero for that direction.

The incoming power at a surface element dA with normal ω_a is equal to the incoming irradiance times the projected area:

$$\Phi_0 = E_0\ \cos\theta_0'\ dA,$$

where $\cos\theta_0'$ is the cosine of the angle between the normal and the incoming direction. The amount of power that is reflected and refracted is determined by the Fresnel factor $F(\cos\theta_0', \eta)$ [2]. Indeed, a fraction F of the power is reflected while a portion $(1-F)$ is refracted. The radiance reflected is by definition the power reflected per solid angle and foreshortened area. To get the total radiance reflected into direction ω_r, we multiply the radiance reflected by a point of the surface with normal ω_a by the Beckmann probability function defined in Equation 17:

$$u_r = \frac{F\ E_0\ \cos\theta_0'\ P(\omega_a)\ d\omega_a}{\cos\theta_r d\omega_r}.$$

The solid angles $d\omega_r$ and $d\omega_a$ are not independent. This can be understood intuitively: by varying the normal in the cone $d\omega_a$ we get a corresponding variation around the reflected direction ω_r. The

size of this variation is exactly the factor which relates the two solid angles. The precise relation between them was cited by Torrance and Sparrow [22]:

$$d\omega_r = 4 \cos\theta_0' \; d\omega_a.$$

Nayar provides an elegant geometric proof of this result [15]. In Appendix B we give an alternative proof which easily generalizes to the case of refraction to be discussed below. Consequently, the BRDF for a surface of roughness σ and with ratio of indices of refraction η is:

$$r = \frac{F(\cos\theta_0', \eta) \; P(\omega_a)}{4 \; \cos\theta_r \; \cos\theta_0}.$$

This result, when multiplied by a shadowing function, is essentially the Cook-Torrance BRDF.

We now derive the BTDF in a similar fashion. As in the reflected case, the total radiance refracted into a direction ω_t is given by:

$$u_t = \frac{(1-F) \; E_0 \; \cos\theta_0' \; P(\omega_a) \; d\omega_a}{\cos\theta_t \; d\omega_t}.$$

The relation between the solid angles $d\omega_t$ and $d\omega_a$ is, however, very different. At first we did not pay too much attention to this relationship and simply assumed $d\omega_a = d\omega_t$. But when we compared our analytical model with a Monte Carlo simulation for validation, we found large discrepancies. Finally, after a careful analysis of other BRDF derivations [4, 25] we realized the importance of this relation. In Appendix B we prove that:

$$d\omega_t = \frac{\left(\cos\theta_0' - \sqrt{\cos^2\theta_0' + \eta^2 - 1}\right)^2}{\eta\sqrt{\cos^2\theta_0' + \eta^2 - 1}} \; d\omega_a = G(\cos\theta_0', \eta) \; \cos\theta_0' \; d\omega_a.$$

It is interesting to note that for $\eta = 1$ this factor is zero, i.e., when there is no surface, light travels unperturbed in a straight line. With this factor the BTDF is equal to:

$$t = \frac{(1 - F(\cos\theta_0', \eta)) \; P(\omega_a)}{\cos\theta_t \cos\theta_0 \; G(\cos\theta_0', \eta)}.$$

This last expression is the main result of this section: a new BTDF model for an isotropic rough surface. We also multiply this function by the shadowing function proposed by van Ginneken at al. [25]. We prefer this shadowing function over the one used by Cook and Torrance [4] since it is consistent with the underlying model for the surface.

The BRDF and the BTDF are shown for different ratios of indices of refraction η and roughness values σ in Figure 5. The top figure corresponds to a ratio $\eta = 1.4$ which is that of skin. These plots correspond to the functions r_{12}, t_{12}, r_{21} and t_{21} of our skin model. As mentioned above we have validated our derivation using a Monte Carlo simulation. Whether they are a good model for rough surfaces is another matter to be settled by experiment. At least, Cook and Torrance reported good agreement with experiment for the function r_{12} [4].

5 The Skin Shader

The main motivation behind our work was to create good skin shaders. It is clear that our illumination model has many other applications. For example, Hanrahan and Krueger used their model

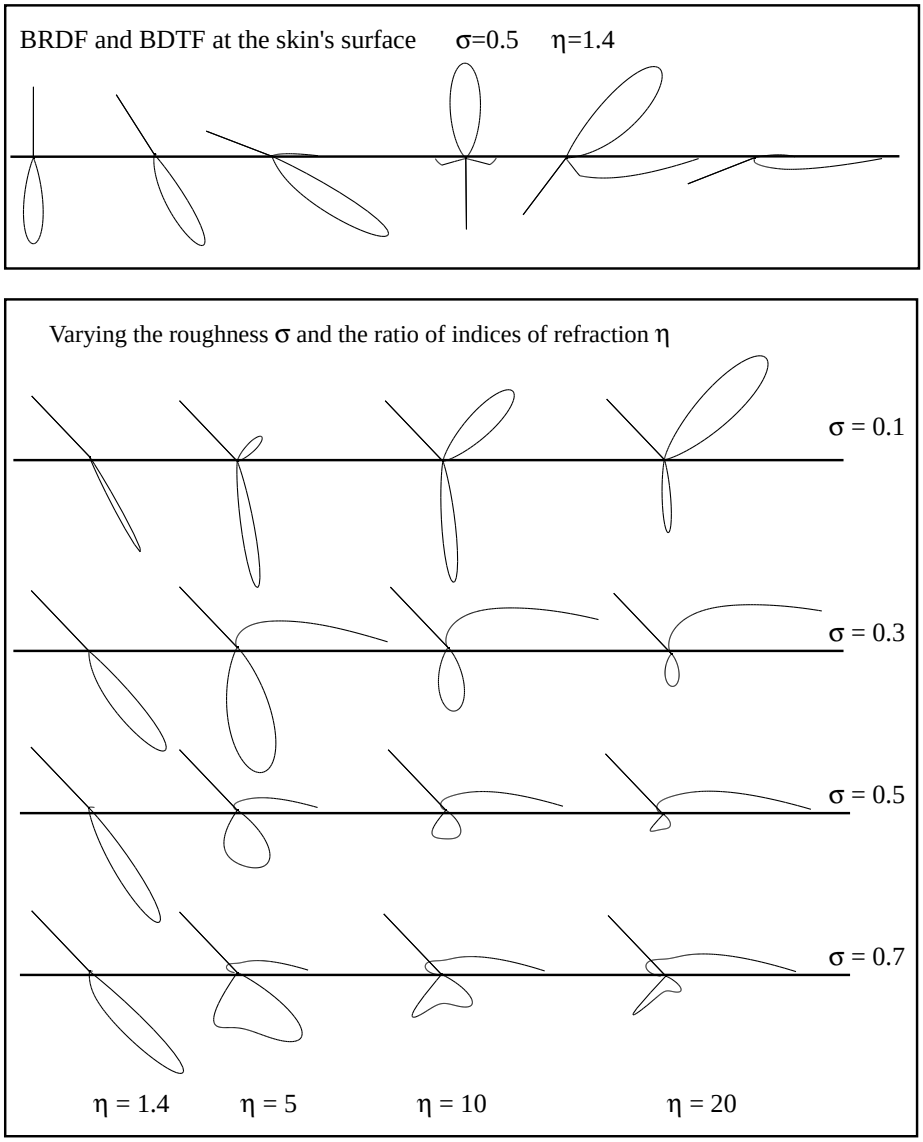

Figure 5: Our new BRDFs and BTDFs for a rough surface. The distributions are rescaled to fit in the figure.

parameter	type	typical values
epidermis	transparency (RGB)	depends the race
dermis albedo	color (RGB)	$(0.993, 0.979, 0.943)$
dermis anisotropy	color (RGB)	$(0.860, 0.854, 0.823)$
surface roughness	scalar	$0.1 - 0.9$

Table 2: Parameters of the skin shader.

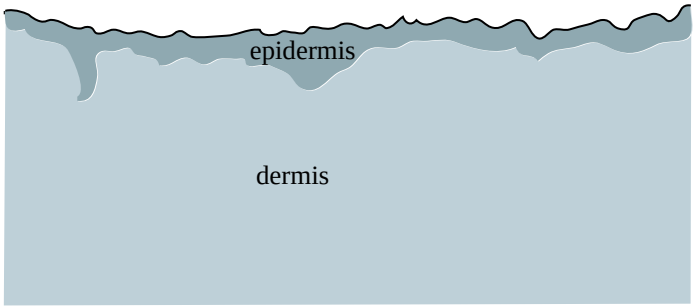

Figure 6: The skin is composed of a rough surface, the epidermis and the dermis. Most of the scattering occurs in the dermis.

to render leaves [5]. As shown in Figure 6, human skin consists of a rough surface and two layers below it: the epidermis and the dermis. The epidermis is a thin layer just below the skin's surface which only scatters weakly and mainly absorbs light. This layer determines the skin's general tone and corresponds to someone's "race". Below the epidermis is the dermis where all the scattering occurs. This layer is almost completely opaque ($T = 0$). The scattering there is characterized by a high albedo ($\Omega \approx 1$) and high forward scattering ($g \approx 0.8$). The shape of the distribution of reflected light depends only on the scattering in the dermis. The effect of the epidermis is simply to scale this distribution. Table 2 lists the parameters of our model. We used the precomputed data mentioned in Section 3.3 to evaluate our shader. We employed a simple quadri-linear interpolation for parameter values different from the ones listed in Table 1. Consequently, all of these parameters can be smoothly texture mapped to achieve many different effects.

We have implemented our reflection model as a shader plugin in our animation software MAYA. The plugin is available for free on our company's web page[1]. The web page also provides more information on the parameters of our skin shader. Several of our customers have recently started to use our shader in production with good results.

Figure 7 shows several examples of human heads rendered using our new skin shader. Figure 7.(a) compares our model (right) to a Lambert shader (left) and the Hanrahan-Krueger (HK) model (center). Our model seems to be a blend between these two models, which is consistent with the plots in Figure 4. Unfortunately, the comparison is necessarily very vague. Indeed, we manually tried to find a set of parameters for both the Lambert shader and the HK model which was as close as possible to our results. In particular, we had to "brighten up" the HK model since it assumes single-scattering. Figure 7.(b) shows our model illuminated by different area light sources. Notice also that we texture mapped both the albedo and the roughness of the lips. Figure 7.(c) is similar for a male head. Finally 7.(d) demonstrates a non-photorealistic application of our shader (notice that the surfaces have been bump mapped).

6 Conclusions and Future Work

In this paper, for the first time, we compute the reflection and the transmission of light through a skin layer bounded by rough surfaces. We achieved this through a discretization of the equation of radiative transfer. We were able to efficiently solve the discrete problem using Fourier transforms

[1] `http://www.aliaswavefront.com` by following "community" and "Download".

(a) Comparison of our shader (right) with a Lambertian shader(left) and the Hanrahan-Krueger model (center)

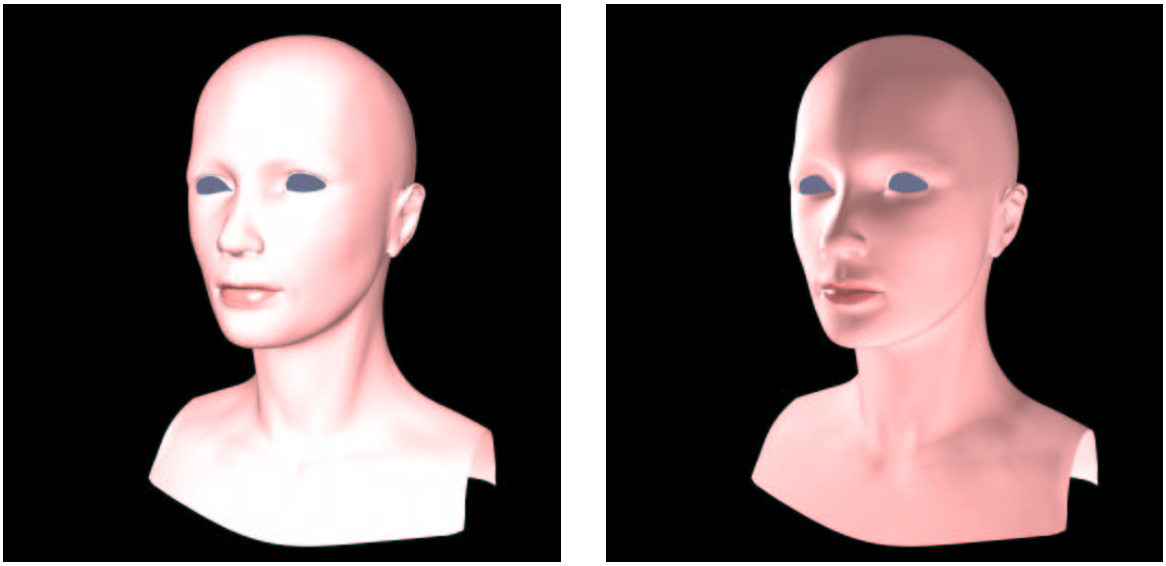

(b) Head under different lighting conditions. Flash-like area source (left) and two area light sources (right)

(c) Another head model with lips and freckles texture mapped.

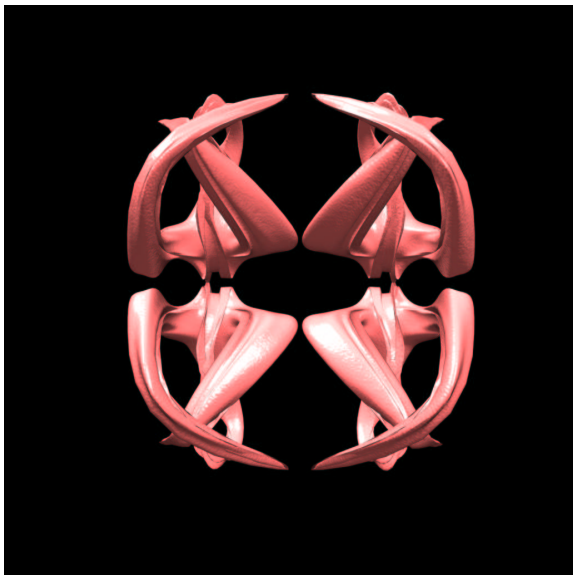

(d) Non-photorealistic application of our model.

Figure 7: Renderings created using our new skin shader.

and eigenanalysis of the scattering matrix. Our model takes into account multiple anisotropic scattering and also handles reflections and refractions at the rough boundaries. To the best of our knowledge a model of this generality has not appeared before in computer graphics or in any of the related fields such as the atmospheric sciences. Our model is therefore of potential interest to these other fields as well. We have precomputed the distributions of reflected and transmitted light for different parameters and used an approximation of that data to build a skin shader. Also, for the first time we derive an analytical model for the Bidirectional Transmittance Distribution Functions (BTDFs) for a rough surface following earlier derivations for the Bidirectional Reflectance Distribution Function.

We have compared our solutions for a subset of our parameters with the output of more expensive Monte Carlo simulations. There was good agreement in each case. We are therefore confident that we have solved the physical formulation of the problem. The question of whether our models match reality has to be settled by comparing them with experimental data. We found a general agreement with the Cornell data [12], however, we feel that more comparisons are needed. Assuming our solver to be bug-free, it would be interesting if there were large discrepancies between our model and experiment. This would suggest that the linear transport theory is perhaps inadequate for this problem. On the practical side, our animators appreciated our new skin shader as it gave them an effect previously possible only with texture mapped Phong-like models. Possible future effects they have requested include "glowing ears", better skin bump-maps, tiny hairs, etc, which are of course hard to model using a shader alone. We are currently investigating how to achieve these effects.

There are many obvious extensions to our model. First, it is easy to include different scattering layers in our model, and our implementation can handle different layers. However, we found that one layer was good enough for the skin shader. To keep this paper as readable as possible, we decided not to add another index referring to the layers. The model can also be extended to handle anisotropic surfaces: simply use Fourier series instead of Cosine series for the azimuthal dependence of the radiances.

We intend to make our data publicly available in the hope that it might lead someone to find a better approximation scheme. Ideally, we would like to have a simple analytical model that fits the data. This would be of great practical and theoretical interest to many applied fields.

A Details: Angular Discretization

In this appendix we provide the missing details of Section 2.3 that lead to explicit expressions for the matrices $\mathbf{M}_k$.

First, we expand the phase function into a cosine series as well:

$$p(\omega', \omega) = \sum_{k=0}^{N} p_k(\mu', \mu) \cos k(\phi - \phi'), \tag{18}$$

where the p_k are functions of the anisotropy factor g and the associated Legendre functions as shown in Appendix C. If we substitute Equations 7 and 18 into Eq. 4 we get the following $N + 1$ equations ($k = 0, \cdots, N$):

$$\mu \frac{d}{d\tau} u_k(\mu) = u_k(\mu) - \Omega_k \int_{-1}^{+1} p_k(\mu', \mu)\ u_k(\mu')\ d\mu', \tag{19}$$

where

$$\Omega_k = \Omega \frac{(1+\delta_{0,k})}{4}$$

and $\delta_{i,j}$ is the Kronecker symbol. We now discretize the problem further by approximating the integrals in Equations 19 using a quadrature:

$$\int_{-1}^{+1} f(\mu')\, d\mu' \approx \sum_{m=1}^{M} w_m \left\{ f(-\mu_m) + f(\mu_m) \right\},$$

where w_m are the weights and $\mu_m \geq 0$ are the ordinates of the quadrature. With this approximation Equation 19 becomes a set of linear equations:

$$\mu_n \frac{d}{d\tau} u_k(\mu_n) = u_k(\mu_n) - \Omega_k \sum_{m=1}^{M} w_m \left\{ p_k(-\mu_m, \mu_n) u_k(-\mu_m) + p_k(\mu_m, \mu_n) u_k(\mu_m) \right\}$$

$$-\mu_n \frac{d}{d\tau} u_k(-\mu_n) = u_k(-\mu_n) - \Omega_k \sum_{m=1}^{M} w_m \left\{ p_k(-\mu_m, -\mu_n) u_k(-\mu_m) + p_k(\mu_m, -\mu_n) u_k(\mu_m) \right\}.$$

Since $p_k(-\mu_m, \mu_n) = p_k(\mu_m, -\mu_n)$ and $p_k(\mu_m, \mu_n) = p_k(-\mu_m, -\mu_n)$ we introduce the following two $M \times M$ matrices:

$$\begin{aligned} (A_k)_{n,m} &= \left(\Omega_k w_m p_k(\mu_m, \mu_n) - \delta_{n,m}\right)/\mu_n \quad \text{and} \\ (B_k)_{n,m} &= \Omega_k w_m p_k(-\mu_m, \mu_n)/\mu_n. \end{aligned}$$

Consequently, recalling the vector notations introduced in Section 2.3:

$$\mathbf{M}_k = \begin{pmatrix} -\mathbf{A}_k & -\mathbf{B}_k \\ \mathbf{B}_k & \mathbf{A}_k \end{pmatrix}.$$

B Relating $d\omega$ to $d\omega_a$

Computing the relationship between the two differentials $d\omega_a$ and $d\omega$ is mathematically equivalent to computing the Jacobian of the change of coordinates $\omega_a \rightarrow \omega$. In this appendix we compute the Jacobians for both the reflected and the refracted solid angles. We compute the change of coordinates in three steps:

$$\omega_a \longrightarrow (x_a, y_a) \longrightarrow (x, y) \longrightarrow \omega.$$

The relation between the spherical and cartesian coordinates is well known and given by

$$dx_a\, dy_a = \mu_a\, d\omega_a \quad \text{and} \quad dx\, dy = \mu\, d\omega.$$

Following the approach of Nayar et al. [15] we assume without loss of generality that the solid angle of the normal $d\omega_a$ is centered along the normal $(0, 0, 1)$. We also assume that the source is coming from the direction $(\mu_0, 0)$, or in cartesian coordinates $\mathbf{v}_0 = (\sqrt{1-\mu_0^2}, 0, \mu_0)$. See Figure 8. Let

$$\mathbf{n}(x_a, y_a) = (x_a, y_a, \sqrt{1 - x_a^2 - y_a^2})$$

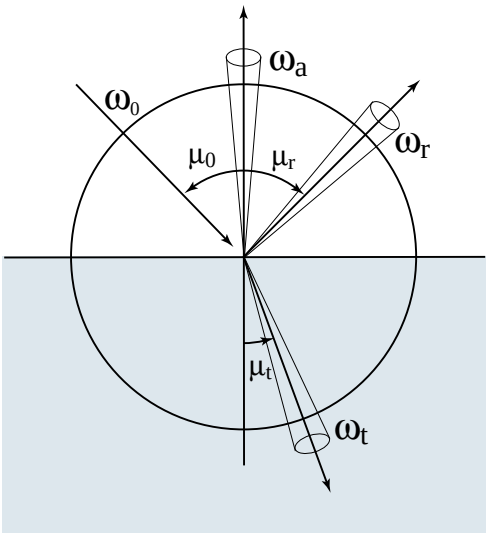

Figure 8: Solid angles involved.

be a normal in $dx_a\ dy_a$. Then the reflected and refracted directions are equal to

$$\begin{aligned} \mathbf{r} &= 2(\mathbf{n}\cdot\mathbf{v}_0)\mathbf{n} - \mathbf{v}_0 \quad \text{and} \\ \eta\mathbf{t} &= \left(\mathbf{n}\cdot\mathbf{v}_0 - \sqrt{(\mathbf{n}\cdot\mathbf{v}_0)^2 + \eta^2 - 1}\right)\mathbf{n} - \mathbf{v}_0, \end{aligned}$$

respectively. The transformation from the normal to the reflected vector corresponds to a change of coordinates $(x_a, y_a) \rightarrow (x, y)$, where

$$\begin{aligned} x &= 2(\sqrt{1-\mu_0^2}x_a + \mu_0\sqrt{1-x_a^2-y_a^2})x_a - \sqrt{1-\mu_0^2} \\ y &= 2(\sqrt{1-\mu_0^2}x_a + \mu_0\sqrt{1-x_a^2-y_a^2})y_a. \end{aligned}$$

The Jacobian of this change of coordinates at $(x_a, y_a) = (0, 0)$ is easily calculated to be equal to:

$$J = \begin{vmatrix} \frac{\partial x}{\partial x_a} & \frac{\partial x}{\partial y_a} \\ \frac{\partial y}{\partial x_a} & \frac{\partial y}{\partial y_a} \end{vmatrix} = \begin{vmatrix} 2\ \mu_0 & 0 \\ 0 & 2\ \mu_0 \end{vmatrix} = 4\ \mu_0^2.$$

Therefore,

$$\mu_0 d\omega = dxdy = 4\mu_0^2 dx_a dy_a = 4\mu_0^2 d\omega_a.$$

In other words,

$$d\omega = 4\mu_0\ d\omega_a,$$

which agrees with Nayar's result [15]. Our derivation might seem unnecessarily complicated compared to that of Nayar [15]. However, our derivation has the merit that it can easily be applied to the refraction problem as well. The Jacobian of the change of coordinates corresponding to the refraction at $(0, 0)$ is equal to

$$\eta^2 J = \begin{vmatrix} \mu_0 - \mu_t & 0 \\ 0 & \mu_0 - \mu_t \end{vmatrix} = (\mu_0 - \mu_t)^2,$$

where

$$\mu_t = \sqrt{\mu_0^2 + \eta^2 - 1}$$

is the cosine of the refracted direction. Again we have the chain of relations

$$\frac{1}{\eta}\mu_t \, d\omega = dxdy = \frac{1}{\eta^2}\left(\mu_0 - \mu_t\right)^2 \, dx_a dy_a = \frac{1}{\eta^2}\left(\mu_0 - \mu_t\right)^2 \, d\omega_a.$$

Therefore,

$$d\omega = \frac{\left(\mu_0^2 - \mu_t\right)^2}{\eta\mu_t} \, d\omega_a,$$

as advertised in Section 4.

C Representation of the Phase Function

The Henyey-Greenstein Phase function has the nice property that it can be expanded explicitly in a cosine series given by Equation 18. The coefficients in the expansion are expressed in terms of the associated Legendre functions [3]. This explains why this phase function is so popular in the radiative transfer literature. The expansion follows from the following result [6]:

$$p(\cos\gamma) = \sum_{k=0}^{N}(2k+1)g^k P_k(\cos\gamma),$$

where P_k is the Legendre polynomial of degree k. From a well known relation between the Legendre polynomials and the associated ones[2], we see that the coefficients in the expansion of Equation 18 are given by:

$$p_k(\mu',\mu) = (2-\delta_{0,k})\sum_{n=k}^{N}(2n+1)g^n\frac{(n-k)!}{(n+k)!}P_n^k(\mu')P_n^k(\mu),$$

where $P_n^k(x)$ are the *associated Legendre functions* [19].

D Discrete Representation of the BRDF and BTDF

Let $\rho(\omega',\omega)$ be one of our BRDFs or BTDFs. We then want to compute the coefficients ρ_k in the cosine series:

$$\rho(\omega',\omega) = \sum_{k=0}^{N}\rho_k(\mu',\mu)\cos k(\phi-\phi').$$

Unlike the phase function in Appendix C, we cannot express these coefficients analytically for the BRDF and BTDF derived in Section 4. For the given set of ordinates $\mu_1,\cdots,\mu_M$ we approximate the integrals:

$$I_k(\mu_n,\mu_m) = \int_0^{2\pi}\rho(\pm\mu_n,0;\pm\mu_m,\phi)\ \cos k\phi \, d\phi,$$

for $k = 0,\cdots,N$ and $n,m = 1,\cdots,M$. The signs in the integrand depend on the BRDF/BTDF being computed. The discrete representation of the linear operators associated with ρ are then given by matrices $\mathbf{L}_k$ whose elements are

$$(L_k)_{n,m} = I_k(\mu_n,\mu_m).$$

[2]This relation was used in [9], for example.

E Computation of Eigenvalues and Eigenvectors of Eq. 9

We seek a $2M$-dimensional vector $(\mathbf{a}, \mathbf{b})^T$ and a scalar λ that satisfy

$$\lambda \begin{pmatrix} \mathbf{a} \\ \mathbf{b} \end{pmatrix} = \begin{pmatrix} -\mathbf{A} & -\mathbf{B} \\ \mathbf{B} & \mathbf{A} \end{pmatrix} \begin{pmatrix} \mathbf{a} \\ \mathbf{b} \end{pmatrix}.$$

Equivalently,

$$\begin{aligned} \lambda(\mathbf{a}+\mathbf{b}) &= (\mathbf{A}-\mathbf{B})(\mathbf{b}-\mathbf{a}) \\ \lambda(\mathbf{b}-\mathbf{a}) &= (\mathbf{A}+\mathbf{B})(\mathbf{a}+\mathbf{b}) \end{aligned}$$

hence

$$\lambda^2(\mathbf{a}+\mathbf{b}) = (\mathbf{A}-\mathbf{B})(\mathbf{A}+\mathbf{B})(\mathbf{a}+\mathbf{b}).$$

Thus we have reduced the problem to size M. We can solve this problem using standard numerical methods to get M eigenvalues $\alpha_1, \cdots, \alpha_M > 0$ and M eigenvectors $\mathbf{e}_1, \cdots, \mathbf{e}_M$. Now, let $\lambda_n = \sqrt{\alpha_n}$ and $\lambda_n \mathbf{f}_n = -(\mathbf{B}+\mathbf{A})\mathbf{e}_n$, and

$$\mathbf{v}_n^+ = \frac{1}{2}(\mathbf{e}_n + \mathbf{f}_n) \quad \text{and} \quad \mathbf{v}_n^- = \frac{1}{2}(\mathbf{e}_n - \mathbf{f}_n).$$

One can verify that these definitions provide eigenvalues and eigenvectors for our original problem:

$$\lambda_n \begin{pmatrix} \mathbf{v}_n^+ \\ \mathbf{v}_n^- \end{pmatrix} = \begin{pmatrix} -\mathbf{A} & -\mathbf{B} \\ \mathbf{B} & \mathbf{A} \end{pmatrix} \begin{pmatrix} \mathbf{v}_n^+ \\ \mathbf{v}_n^- \end{pmatrix} \quad \text{and} \quad -\lambda_n \begin{pmatrix} \mathbf{v}_n^- \\ \mathbf{v}_n^+ \end{pmatrix} = \begin{pmatrix} -\mathbf{A} & -\mathbf{B} \\ \mathbf{B} & \mathbf{A} \end{pmatrix} \begin{pmatrix} \mathbf{v}_n^- \\ \mathbf{v}_n^+ \end{pmatrix}.$$

These results can be written more compactly using the following matrices:

$$\mathbf{V}^+ = \left(\mathbf{v}_1^+ \cdots \mathbf{v}_M^+\right), \ \mathbf{V}^- = \left(\mathbf{v}_1^- \cdots \mathbf{v}_M^-\right) \quad \text{and} \quad \mathbf{\Lambda}^+ = \mathrm{diag}(\lambda_1, \ldots, \lambda_M).$$

We obtain the following matrices of eigenvectors and eigenvalues:

$$\mathbf{V} = \begin{pmatrix} \mathbf{V}^+ & \mathbf{V}^- \\ \mathbf{V}^- & \mathbf{V}^+ \end{pmatrix} \quad \text{and} \quad \mathbf{\Lambda} = \begin{pmatrix} \mathbf{\Lambda}^+ & \mathbf{0} \\ \mathbf{0} & -\mathbf{\Lambda}^+ \end{pmatrix}.$$

References

[1] P. Beckmann and A. Spizzichino. *The Scattering of Electromagnetic Waves from Rough Surfaces*. Pergamon, New York, 1963.

[2] M. Born and E. Wolf. *Principles of Optics. Sixth (corrected) Edition*. Cambridge University Press, Cambridge, U.K., 1997.

[3] S. Chandrasekhar. *Radiative Transfer*. Dover, New York, 1960.

[4] R. L. Cook and K. E. Torrance. A Reflectance Model for Computer Graphics. *ACM Computer Graphics (SIGGRAPH '81)*, 15(3):307–316, August 1981.

[5] P. Hanrahan and W. Krueger. Reflection from Layered Surfaces due to Subsurface Scattering. In *Proceedings of SIGGRAPH '93*, pages 165–174. Addison-Wesley Publishing Company, August 1993.

[6] J. E. Hansen and L. D. Travis. Light Scattering in Planetary Atmospheres. *Space Science Reviews*, 16:527–610, 1974.

[7] X. D. He. *Physically-Based Models for the Reflection, Transmission and Subsurface Scattering of Light by Smooth and Rough Surfaces, with Applications to Realistic Image Synthesis*. PhD thesis, Cornell University, Ithaca, New York, 1993.

[8] Z. Jin and K. Stamnes. Radiative transfer in nonuniformly refracting layered media: atmosphere-ocean system. *Applied Optics*, 33(3):431–442, January 1994.

[9] J. T. Kajiya and B. P. von Herzen. Ray Tracing Volume Densities. *ACM Computer Graphics (SIGGRAPH '84)*, 18(3):165–174, July 1984.

[10] E. P. F. Lafortune, S-C. Foo, K. E. Torrance, and D. P. Greenberg. Non-Linear Approximation of Reflectance Functions. In *Computer Graphics Proceedings, Annual Conference Series, 1997*, pages 117–126, August 1997.

[11] E. Languénou, K.Bouatouch, and M.Chelle. Global illumination in presence of participating media with general properties. In *Proceedings of the 5th Eurographics Workshop on Rendering*, pages 69–85, Darmstadt, Germany, June 1994.

[12] S. R. Marschner, S. H. Westin, E. P. F. Lafortune, K. E. Torrance, and D. P. Greenberg. Image-based brdf measurement including human skin. *Eurographics Workshop on Rendering*, 1999.

[13] N. Max. Efficient light propagation for multiple anisotropic volume scattering. In *Proceedings of the 5th Eurographics Workshop on Rendering*, pages 87–104, Darmstadt, Germany, June 1994.

[14] C. D. Mobley. A numerical model for the computation of radiance distributions in natural waters with wind-roughened surfaces. *Limnology and Oceanography*, 34(8):1473–1483, 1989.

[15] S. K. Nayar, K. Ikeuchi, and T. Kanade. Surface Reflection: Physical and Geometrical Perspectives. *IEEE Transactions on Pattern Analysis and Machine Intelligence*, 13(7):611–634, July 1991.

[16] NETLIB. The code is publicly available from `http://netlib.org`.

[17] G. N. Plass, G. W. Kattawar, and F. E. Catchings. Matrix operator theory of radiative transfer. 1: Rayleigh scattering. *Applied Optics*, 12(2):314–329, February 1973.

[18] A. A. Prahl, M. J. C. van Gemert, , and A. J. Welch. Determining the optical properties of turbid media by using the adding-doubling method. *Applied Optics*, 32:559–568, 1993.

[19] W. H. Press, B. P. Flannery, S. A. Teukolsky, and W. T. Vetterling. *Numerical Recipes in C. The Art of Scientific Computing*. Cambridge University Press, Cambridge, 1988.

[20] H. E. Rushmeier and K. E. Torrance. The Zonal Method for Calculating Light Intensities in the Presence of a Participating Medium. *ACM Computer Graphics (SIGGRAPH '87)*, 21(4):293–302, July 1987.

[21] K. Stamnes and P. Conklin. A New Multi-Layer Discrete Ordinate Approach to Radiative Transfer in Vertically Inhomogeneous Atmospheres. *Journal of Quantum Spectroscopy and Radiative Transfer*, 31(3):273–282, 1984.

[22] K. E. Torrance and E. M. Sparrow. Theory for Off-Specular Reflection From Roughened Surfaces. *Journal of the Optical Society of America*, 57(9):1105–1114, September 1967.

[23] V. V. Tuchin. Light scattering study of tissue. *Physics - Uspekhi*, 40(5):495–515, 1997.

[24] M. J. C. van Gemert, S. L. Jacques, H. J. C. M. Sterenborg, and W. M. Star. Skin optics. *IEEE Transactions on Biomedical Engineering*, 36(12):1146–1154, December 1989.

[25] B. van Ginneken, M. Stavridi, and J. J. Koenderink. Diffuse and specular reflectance from rough surfaces. *Applied Optics*, 37(1):130–139, January 1998.